Modeling investigation of thermal insulation approaches for Low Heat Rejection Diesel Engines using a Conjugate Heat Transfer Model Journal

Adèle Poubeau, Arthur Vauvy, Florence Duffour, Jean-Marc Zaccardi, Gaetano De Paola, Marek Abramczuk

Modeling investigation of thermal insulation approaches for Low Heat Rejection Diesel Engines using a Conjugate Heat Transfer Model

Adèle Poubeau[1], Arthur Vauvy[1], Florence Duffour[1], Jean-Marc Zaccardi[1], Gaetano de Paola[1] and Marek Abramczuk[2]

Abstract

Heat losses through combustion chamber walls are a well-known limiting factor for the overall efficiency of internal combustion engines. Thermal insulation of the walls has the potential to decrease substantially these heat losses. However, evaluating numerically the effect of coating and of its location in the combustion chamber and then design an optimized combustion system requires the use of high fidelity engine models. The objective of this paper is to present the whole workflow implying the use of three-dimensional computational fluid dynamics (CFD) techniques with conjugate heat transfer (CHT) models to investigate the potential benefits of a coating on a passenger car Diesel engine. First, the baseline combustion system is modeled, using CHT models to solve in a coupled simulation the heat transfers between the fluid in the intake and exhaust lines and in the combustion chamber on one hand, and the solid piston, head and valves on the other hand. Based on this setup, a second simulation is performed, modeling a thermo-swing insulation on all combustion chamber walls by a contact resistance, neglecting its thermal inertia to keep a manageable computational cost. Results show a decrease of 3.3% in fuel consumption with an increase in volumetric efficiency. However, decoupled 1D/3D simulations highlight the inaccuracy of these results and the necessity to model the coating thermal inertia, as they show an over-estimation of the heat insulation rate and, consequently, of the gain in fuel consumption (-2.1% instead of -1.6%), for a coating on the piston with no thermal inertia.

Keywords

CFD, Conjugate Heat Transfer, Temperature swing, thermal insulation, efficiency, heat loss

Introduction

In a context where improving efficiency of Diesel engines while limiting pollutant emission formation is crucial for car industry, the reduction of heat losses through the combustion chamber walls, which account for 14-17% of the injected fuel energy[1,2], has been the object of numerous studies over the last decades. The investigation of the potential of Thermal Barrier Coatings (TBC) to improve insulation of the combustion chamber was initiated in the 80s. The objective was to go towards a Low Heat Rejection Engine (LHRE), a term generally referring to the thermal insulation of the combustion chamber using ceramic coatings. A large number of numerical and experimental studies were performed on this topic[1,3–14], giving often contradictory or inconclusive results. An important limitation of this type of coating material, the most common being the partially-stabilized zirconia (PSZ), was a decrease in volumetric efficiency[15,16]. Indeed, due to their relatively high heat capacity, the insulated wall was remaining at a high temperature during the entire cycle, causing an increase in intake air temperature. A way to tackle this issue was recently proposed by Toyota Central R&D Labs and Toyota Motor Corporation[17–21]. Their Thermo-Swing Wall Insulation Technology (TSWIN) uses anodized aluminum with silica filler as a TBC for the piston. In addition to its low thermal conductivity, this material also has a low heat capacity: its temperature follows

closer the fluctuation of in-cylinder gas temperature, offering heat insulation during the combustion phase while limiting or preventing air heating during intake. This TBC featuring a thermal swing, and applied on the crown area of the piston of their 2.8L ESTEC 1 GD-FTV engine, ensures an increase in efficiency up to 2%[17]. These orders of magnitude of gains were very recently confirmed by measurements on a four-cylinder turbocharged Diesel engine using zirconia coating[22].

Current research efforts continue in this direction. If surface temperature and heat flux measurements are crucial to characterize the efficiency of a coating[15,23–25], simulations remain a convenient tool to evaluate a large range of coating materials and optimize their thickness and location. Zero-dimensional and one-dimensional platforms have been widely implemented[16,26]. Three-dimensional simulations have been used in association to these platforms[17,27] or in addition to experiments in order to offer a better comprehension of the interactions between TBC and

[1]IFP Energies nouvelles, Institut Carnot IFPEN TE., France
[2]Renault, France

Corresponding author:
Adèle Poubeau, IFPEN, 1-4 Avenue du Bois Préau, 92852 Rueil-Malmaison, France.
Email: adele.poubeau@ifpen.fr

in-cylinder gas aerodynamics[18,24]. However, a coupling between 3D simulations of the reactive fluid on one hand and of conduction in the solid parts of the engine on the other hand, known as Conjugate Heat Transfer (CHT), appears as the most promising technique for TBC evaluation. By solving heat transfer between fluid and solid parts while accounting for 3D effects such as flame/wall interactions, these simulations can offer a local prediction of the coating effect on heat losses, resulting in a finer evaluation of the TBC effect on the engine performance and pollutant emissions. This technic also allows optimization of the combustion system characteristics (including spray orientation or bowl geometry) along with the TBC (location or thickness).

Integrated in-cylinder/CHT methodologies have been the object of recent works. In particular, an iterative loop of decoupled in-cylinder and CHT simulations was implemented[28], allowing to represent the coupling between in-cylinder processes, the solid components (head, valves, piston) and coolant circuits of a Diesel engine. This approach gave good comparison to experimental results. Another technique consists in solving a coupled simulation between fluid and solid parts. This requires the use of particular methodologies to overcome the impact of the large difference in time-scales between the fluid and solid parts on the computational cost. Such a method is implemented in the CFD software CONVERGE. Previous studies applied this approach to solve CHT on a Diesel piston engine[29], or on the cylinder head of a spark-ignition engine[30]. Comparison with temperature measurements in the solid showed good results. This CHT methodology seems particularly promising for the evaluation of a coating efficiency. It was indeed applied in previous work[29] to model the impact of TBC on the piston on heat losses. In this context, the first objective of this work is to assess the coupled in-cylinder/CHT methodology for coating application, by applying it to a 3D-CFD simulation with thermal simulation of the piston and engine head for a single-cylinder Diesel engine. The second objective is to evaluate the maximum gain to be expected from an innovative coating material by applying it on the entire surface of the combustion chamber. This paper is organized as follows: a description of the engine and operating conditions is given, followed by details about the numerical setup. Then a 3D CHT simulation of the baseline setup without coating is presented. The last section focuses on thermal insulation aspects, with an investigation of the selected coating material using a 1D approach, followed by its application in a 3D CHT simulation. The results are then analyzed and supplemented by extra 1D and 3D simulations.

Engine overview and operating conditions

The experimental setup consists in a single-cylinder Diesel engine. Engine characteristics and details about the operating conditions are listed in Table 1. The conditions correspond to a mid-load operating point.

Table 1. Engine characteristics and operating conditions. BBDC: before bottom dead center; ATDC: after top dead center; ABDC: after bottom dead center.

Engine characteristics	
Number of cylinder	1
Number of valves	4
Stroke	88 mm
Bore	85 mm
Compression ratio	16:1
Exhaust valve open	60 BBDC@ 0.2 mm lift
Exhaust valve close	0 ATDC @ 0.2 mm lift
Intake valve open	0 ATDC @ 0.2 mm lift
Intake valve close	30 ABDC @ 0.2 mm lift

Injector	
Number of holes	8
Permeability	320cc/30s/100bar
Opening angle	155
Injection pressure	2000 bar
Injection strategy	1 pilot + 1 main
Injected mass	2.4 + 30.4 mg

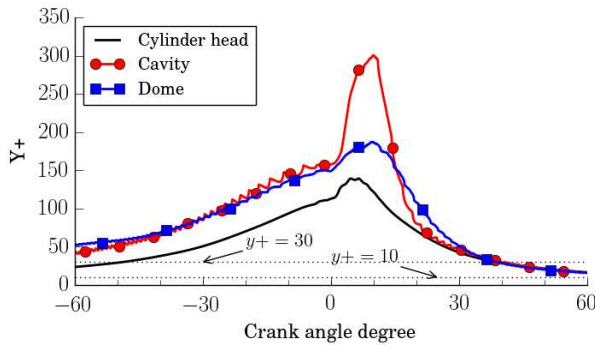| Operating conditions	
Engine speed	2500 rpm
IMEP	12 bar
EGR	23%
Equivalence ratio	0.67
Intake pressure	2.1 bar
Intake temperature	315 K

Numerical setup

The 3D CHT-RANS simulations presented in the framework of this paper were performed using the solver CONVERGE v2.4[31]. The following sections present the gas modeling and CHT methodologies implemented in this work.

Two-phase flow modeling strategy

Combustion is modeled by the 3 Zone Extended Coherent Flame Model (ECFM3Z) model[32]. It has been developed based on the ECFM model[33], in order to account for perfectly, partially mixed and also unmixed combustion, these three regimes being encountered in Diesel engines. It relies on a flame surface density equation which takes into account the wrinkling of the flame front surface by turbulent eddies, and on a conditioning averaging technique allowing precise reconstruction of local properties in fresh and burned gases. To model diffusion flames and mixing processes, each computational cell is split into three mixing zones: a pure fuel zone, a pure air and residual gases zone, and a mixed zone (where the ECFM model is applied). A mixing model allows progressive mixing of the initially unmixed fuel and air.

The Tabulated Kinetics of Ignition (TKI) model[34,35], accounts for auto-ignition. It relies on tabulated auto-ignition parameters deduced from detailed chemistry calculations. In particular, the reaction rate due to auto-ignition is deduced from linear interpolation in a lookup table for local conditions of mean pressure, fresh gases temperature, fuel/air equivalence ratio, EGR volume fraction and auto-ignition progress variable. In the present study, the TKI table was

Figure 1. Evolution of surface averaged y+ on cylinder head, piston cavity and piston dome during compression and combustion phases.

Figure 2. Fluid and solid parts involved in the 3D CHT simulation.

generated using the Chalmers mechanism for n-heptane[36], which was used as a chemical surrogate. The implementation of these models in the CFD code CONVERGE was proven to give relevant results for Diesel combustion modeling[37].

The soot mass production within a ECFM3Z computational cell is determined from a single-step competition between formation and oxidation rates based on the Hiroyasu model[38]. For this model, the soot formation rate depends on the formation C2H2 species which is the precursor chosen for soot production. Soot oxidation is modeled using Nagle and Strickland-Constable correlations assuming the soot particles to be spherical and uniform in size. The NOx formation is modeled using an extended Zeldovich mechanism[39].
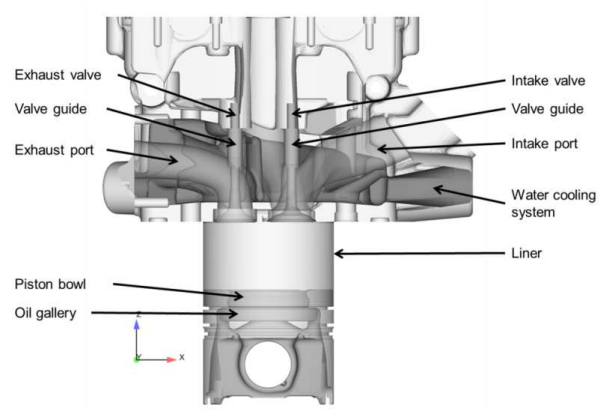
Concerning turbulence, the $k - \epsilon$ RNG model is used, along with a law-of-the-wall approach[40] to model the turbulence kinetic energy and dissipation within the boundary layer. Thermal heat fluxes at the wall boundaries are calculated using the wall heat transfer model of O'Rourke and Amsden[41].

The Diesel spray is modeled using the blob injection approach[42]: the characteristic size of the injected parcels are equal to the effective diameter of the nozzle. The Kelvin-Helmhotz (KH) and Rayleigh-Taylor (RT) instability mechanisms are used to model the spray breakup[31]. The interactions between spray and walls rely on a particle-based approach. In particular, the liquid film transport follows the model of O'Rourke and Amsden[43].

The gaseous computational domain is automatically discretized using the cut-cell Cartesian method implemented in CONVERGE. To ensure sufficient grid refinement during the combustion phase, fixed embedding are used in the liquid spray region and along the walls. The Adaptative Mesh Refinement (AMR) tool is also used to apply a relevant refinement of the grid in the regions of strong gradients of velocity and temperature. Mesh size varies between 0.7 and 1.4 mm. In particular, the size of the cells at the walls were chosen so that the y+ remains larger than 10 close to TDC (as illustrated in Fig. 1), ensuring the validity of the turbulence model[28].

CHT methodology

The CHT model aims at computing heat transfer between the reactive gas and the surrounding engine parts. In CONVERGE, the flow in the fluid region is coupled to heat conduction in the solid. To tackle the issue caused by the disparity in time scales between the fluid and solid, the super-cycling model[29] is used. This approach is based on the observation that the solid is not sensitive to instantaneous variations of the gas aerodynamics. The fluid and solid are solved via a strong coupling for a super-cycling time interval (60 CAD for the present simulations). At the fluid-solid interface, near wall temperatures and heat transfer coefficients (denoted h) are stored at each time step. At the end of each super-cycling interval, the fluid solver is paused and conduction in the solid is solved until convergence, using as boundary conditions the near wall temperatures and heat transfer coefficients, time-averaged over the last 720 CAD of the simulation. The fluid and solid regions are then solved again with a strong coupling, for the next super-cycling interval. These steps are repeated until the solid temperature converges. Overall, only three cycles were necessary to converge the solid temperature (including the first cycle, during which near-wall temperatures and heat transfer coefficients are stored and super-cycling has not yet started).

In the present simulations, the CHT model is applied to the piston and cylinder head (see Fig. 2). A constant temperature boundary condition is assumed for the liner walls. Convective boundary conditions (h and far-field temperature) are imposed on all other outer walls, derived from previous thermal analysis.

To better reproduce the thermal behaviour of the various solids, solid properties (conductivity, density and specific heat) are specified for the piston, engine head, valves, valve guide and valve seats. No contact resistance is modelled at the solid-to-solid interfaces. In particular, contact resistance between the valves and the valve seats, when the valves are closed, are not modelled. This should lead to inaccuracies in the computation of valve surface temperatures, as well as cylinder head temperature. In the solid parts, mesh size varies between 0.7 and 5.6 mm, with a local refinement at the interfaces fluid/solid and solid/solid. If the grid is fine enough to observe accurate heat transfer while keeping the computational cost reasonable, it remains too coarse to simulate temperature variations during the cycle in the near wall cells on the solid parts.

3D Conjugate Heat Transfer simulations without coating

Comparison with experimental data

The results of the last computed cycle are compared to experimental data in Fig. 3 and Fig. 4. In-cylinder pressure signals and apparent heat release rates compare relatively well, as well as values of gross indicated mean effective pressure imep_g and duration of half the combustion process $\Delta\Theta_{50\%}$.

Analysis of heat transfers through chamber walls

To refine the observations, the piston surface was discretized into 3 parts, as illustrated in Fig. 5: top, cavity and dome. Fig. 6 depicts heat losses rate and cumulative heat losses over the entire cycle through these 3 surfaces. The differences between each part result from the non-uniform cooling effect of the oil gallery, as well as internal aerodynamics, determined by the angle and vertical position of injector holes, and the piston geometry. The cavity and the top parts, directly impacted by the flame, represent 48 and 37% of heat losses through the piston respectively, against 15% for the dome. These results suggest that the thermo-physical properties of the coating, its location and thickness have to be optimized along with the combustion system parameters (in particular bowl geometry and injection settings) in order to maximize the benefits.

The normalized cumulative heat losses through all walls of the chamber are presented in Fig. 7. The piston represents half of the heat losses (which is coherent with previous results stating a range of 50-68%[1,2], and the cylinder head almost 20%. It should be reminded that the heat losses through the liner presented here do not result from a CHT simulation: a constant temperature is applied on the surface throughout the cycle, which limits the accuracy of this result.

Thermal insulation modeling

Thermal swing wall insulation

Heat losses from the combustion chamber can be reduced by decreasing the temperature difference between the in-cylinder hot gas and wall surface. This effect can be obtained by adding a layer of insulation material on the wall surface (e.g the piston head, or the cylinder head). However, depending on thermo-physical properties of the material, unwanted effects can be observed. For instance, materials such as zirconium (Y-PSZ, Yttria-Partially Stabilized Zirconia in Fig. 8), with a low thermal conductivity and a relatively high specific heat capacity, increase negative heat transfer (from wall to gas) during intake, resulting in a deteriorated volumetric efficiency and potential impacts on knocking (for SI engines) or pollutants[16,18]. By decreasing the material heat capacity while keeping a low thermal conductivity, the temperature surface follows closer the in-cylinder gas temperature, reducing heat losses during the combustion phase when temperature increases, and maintaining or even increasing volumetric efficiency with similar or lower surface temperature during intake stroke. Such a thermo-swing insulation has been developed by
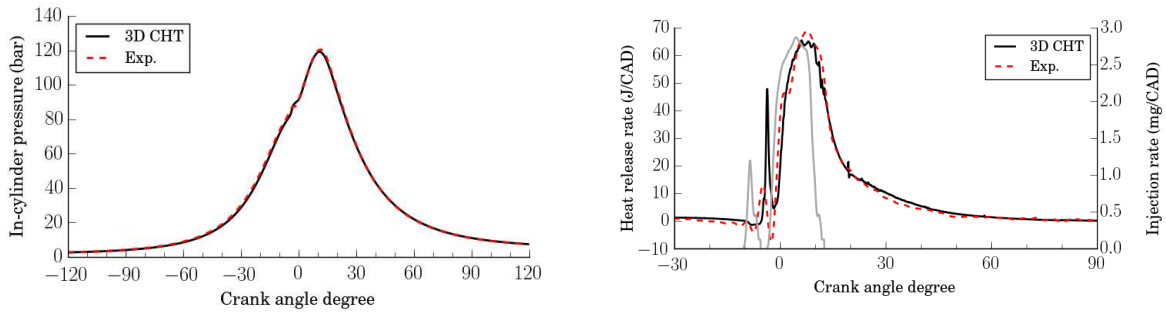
Toyota Central R&D Labs and Toyota Motor Corporation[17]: the SiRPA insulation technology consists in anodized aluminum with silica filler and should ensures up to 2% relative increase in the engine thermal efficiency of a 2.8L ESTEC 1 GD-FTV engine[44]. Its properties are shown in Fig. 8. The insulation material proposed in this study, denoted "Ref." in Fig. 8, follows this principle. Its thermal conductivity is $0.4\ W \cdot m^{-1} \cdot K^{-1}$, and its volumetric heat capacity is $920\ kJ \cdot m^{-3} \cdot K^{-1}$. To offer a first investigation of the gains to be expected with this insulation material, the surface temperature and heat transfer resulting from the use of a thermal barrier were evaluated with a simple one-dimensional computation of heat conduction in the direction perpendicular to the insulated wall[17,45]. The model is described in Fig. 9. A case without thermal insulation is used as a reference. Temperature is evaluated by solving the 1D heat equation in both solids:

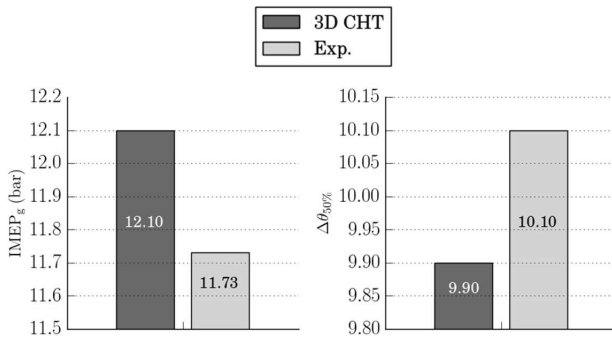$$\frac{\partial T}{\partial t} = \frac{\lambda_k}{\rho_k c_{p,k}} \frac{\partial^2 T}{\partial x^2} \qquad (1)$$

with $k = 1, 2$ designating the thermal insulation and the aluminum respectively, of thickness e and L. This equation was discretized using a first-order, centered finite difference scheme. The interface temperature between the aluminum and the thermal insulation can be easily derived from a surface energy balance equation. On the gas side ($x = 0$), a convective boundary condition is imposed, consisting of the crank-varying, space-averaged in-cylinder gas temperature T_{cyl} and heat transfer coefficient h, obtained from the 3D-CHT simulation presented in the previous section. The convective boundary condition is written so that heat transfers are positive when the gas heats the wall:

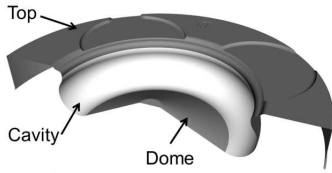$$-\lambda_1 \frac{\partial T}{\partial x} = h(t)\left[T_{cyl}(t) - T(x = 0)\right] \qquad (2)$$

For the simulations of the present section, the heat transfer coefficient was computed based on surface temperature and heat transfer spatially averaged on the piston dome. The length of the aluminum bar L is of the same order of magnitude as the piston thickness close to the dome, about 1.5 cm. On the coolant side, a constant temperature is applied. Its value was tuned so that for the case without insulation layer, the resulting mean surface temperature on the gas side matches those of the 3D-CHT simulation. The boundary conditions remain the same for the cases without and with insulation layer, meaning the effect of coating on gas dynamics is neglected. The 1D model with thermal insulation was applied with the reference coating material, along with SiRPA and Y-PSZ for comparison. Various coating thicknesses e were applied, from 10 to 1000 μm. The impact of insulation thickness on surface temperature is illustrated in Fig. 10 for the reference coating material: as it increases, the average surface temperature increases too, in particular during intake, losing progressively the thermo-swing effect. Beyond $e = 100\mu m$, volumetric efficiency should be degraded. This observation is confirmed by Fig. 11, which depicts the evolution of heat insulation rate against intake gas heat rate, for 5 values of coating thickness: $e = 10, 50, 80, 100$ and $150\ \mu m$ and the 3 materials. Heat insulation rate, or HIR, represents the percentage of reduction in heat losses over a cycle for a coated surface with

Figure 3. In-cylinder pressure (spatially averaged in the chamber) on the left, and apparent heat release rate on the right (with the injection rate imposed in the CFD simulation in grey). The solid line corresponds to 3D CHT results, the dashed line to experimental results.

Figure 4. Comparison of $\mathrm{imep_g}$ (left) and $\Delta\Theta_{50\%}$ (right), for the experimental and numerical results

Figure 5. Discretization of the piston surface.

respect to the baseline wall. It is written:

$$\mathrm{HIR} = 100 \times \frac{\int_{cycle} \dot{Q}_{gas\rightarrow wall}^{alu} - \int_{cycle} \dot{Q}_{gas\rightarrow wall}^{coating}}{\int_{cycle} \dot{Q}_{gas\rightarrow wall}^{alu}} \quad (3)$$

where $\dot{Q}_{gas\rightarrow wall}$ is the rate of heat conduction at the wall surface. Intake gas heat rate, or IGHR, is the percentage of increase in heat transfer from wall to gas during intake[1] for a coated surface with respect to the baseline wall:

$$\mathrm{IGHR} = 100 \times \frac{\int_{intake} \dot{Q}_{gas\rightarrow wall}^{coating} - \int_{intake} \dot{Q}_{gas\rightarrow wall}^{alu}}{\int_{intake} \dot{Q}_{gas\rightarrow wall}^{alu}} \quad (4)$$

A positive value means the gas is heated by the wall during intake. Fig. 11 highlights the compromise to be found between global reduction of heat losses and volumetric efficiency when choosing the insulation thickness. The optimal thickness (in the sense that it maximizes insulation without impacting volumetric efficiency) seems to be around 80 μm for all materials. However, depending on the selected manufacturing process, it might be technically complicated

to apply a coating with a thickness lower than 100 μm. Therefore a thickness of 100 μm was retained for the present study. The 1D simulation shows that a decrease in heat losses of 15% is to be expected, for an increase in gas heating during intake of 10%. However, these results are certainly over-estimated, as they do not take into account the increase in the near-wall gas temperature due to higher surface temperature when insulation is applied.
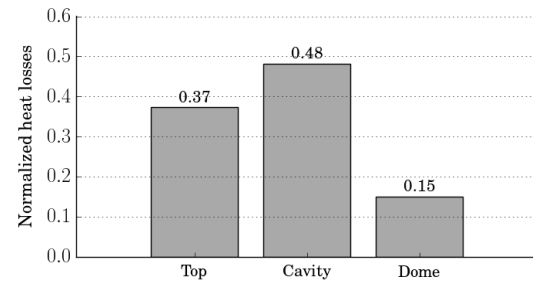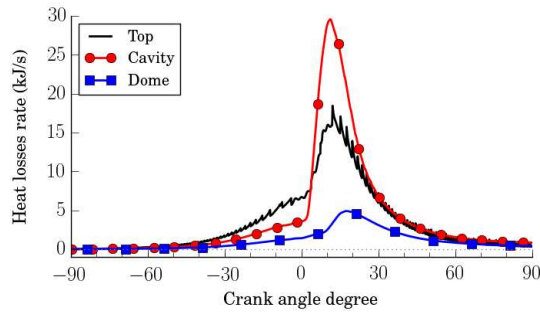
Modeling wall insulation in 3D CHT simulations

The numerical setup of the 3D CHT-RANS is used to evaluate the impact of the reference coating described in the previous section. The objective is to estimate the maximal potential of the coating by applying it on the entire combustion chamber (except the liner): cylinder head, bottom surfaces of the four valves and piston surface. The thickness of the coating, 100 μm, is smaller than the minimum cell size in the chamber. Resolving the TBC would require an extremely fine mesh, thus increasing dramatically the computational cost. Instead, it was decided to neglect the thermal inertia of the coating material and model only the thermal resistance[29], defined as:
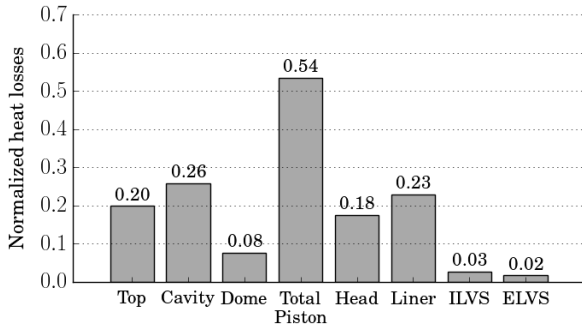
$$R_{TBC} = \frac{e}{\lambda_{TBC}} \quad (5)$$

with e the coating thickness and λ_{TBC} the thermal conductivity. The effect of the TBC on heat losses is illustrated in Fig. 12, depicting heat losses rate and cumulative heat losses over the piston dome, with and without TBC. The reduction of heat losses during the combustion phase is significant (-26% between -10 and 100 CAD). However, during intake, heat losses should be lower for the simulation with TBC, as the coating is expected to warm the fresh gas, which should result in negative heat losses (Fig. 11). However, according to these simulations, this is not the case.
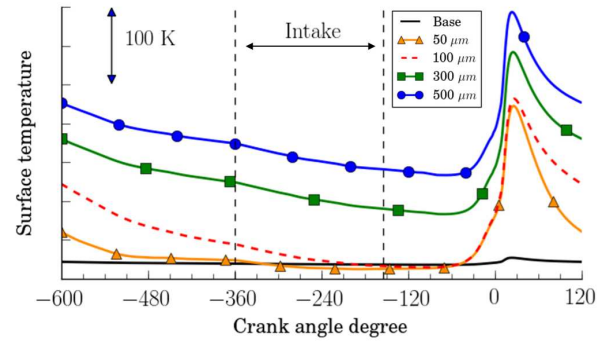
To improve comprehension, Fig. 13 focuses on the impact of coating during intake. It can be noticed that the volume-averaged piston temperature (excluding the surface) decreases by 4.75% with TBC. This is expected, as the coating acts like a barrier and prevents the hot gases of the combustion chamber to heat the piston. As a result, and as the thermal inertia of the TBC is not modelled, heat transfers from wall to gas during intake are lower with the TBC model (-10.8%, following Eq. 4): in-cylinder gases are less heated by the chamber walls (their average temperature
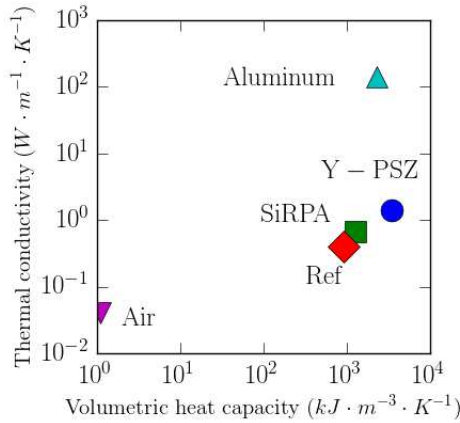
Figure 6. Heat losses rate (left) and normalized heat losses (right) through piston surface.
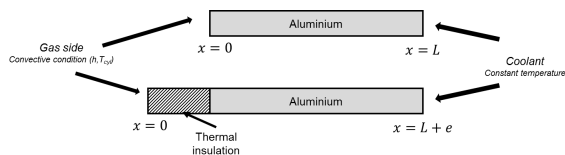

Figure 7. Normalized heat losses through the cylinder walls. ILVS: intake lower valve surface; ELVS: exhaust lower valve surface.
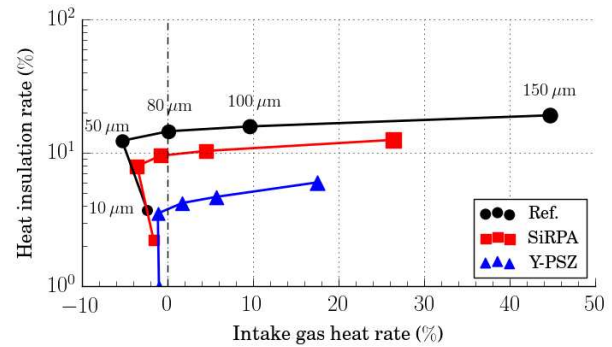

Figure 8. Thermo-physical properties of various insulation materials. "Ref." denotes the reference coating material considered in this study.
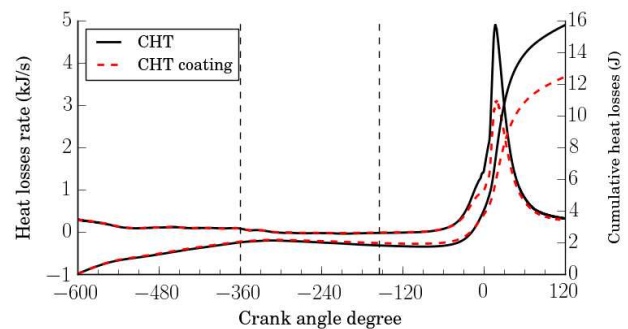

Figure 9. 1D model of an aluminum bar, with and without thermal insulation, along with boundary conditions.

Figure 10. Surface temperature profiles for various thicknesses of the reference coating.

Figure 11. Heat insulation rate against intake gas heat rate for 5 values of insulation thickness and 3 coatings. "Ref." represents the reference coating considered in this study.

Figure 12. Instantaneous (left axis) and cumulative (right axis) heat loss on the piston dome with and without coating (3D CHT simulations).

during intake loses 1%), which results into an increase in in-cylinder mass before SOI (+0.6%). These results would certainly by different by taking into account the thermal inertia of the TBC, as it will be suggested in the last section.

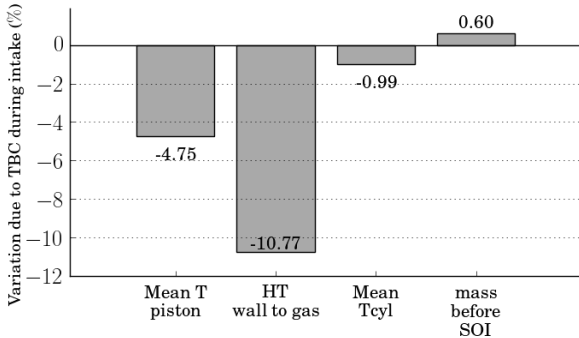For each wall of the combustion chamber, Fig. 14 shows the heat insulation rate compared to the baseline wall (as defined in Eq. 3), and compared to the total decrease in heat

Figure 13. Relative variation due to TBC of mean piston temperature, integrated heat transfer from wall to gas during intake, mean in-cylinder gas temperature during intake and in-cylinder mass (before SOI, start of injection), compared to the baseline.
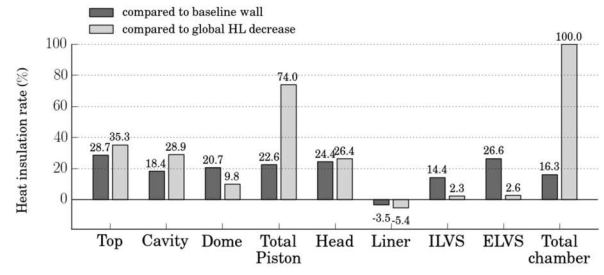
losses in the chamber:

$$\text{HIR}_{\text{tot}} = \frac{100 \times \int_{cycle} \dot{Q}_{gas \to wall}^{alu} - \int_{cycle} \dot{Q}_{gas \to wall}^{coating}}{\sum_{walls} \left[\int_{cycle} \dot{Q}_{gas \to wall}^{alu} - \int_{cycle} \dot{Q}_{gas \to wall}^{coating} \right]} \quad (6)$$
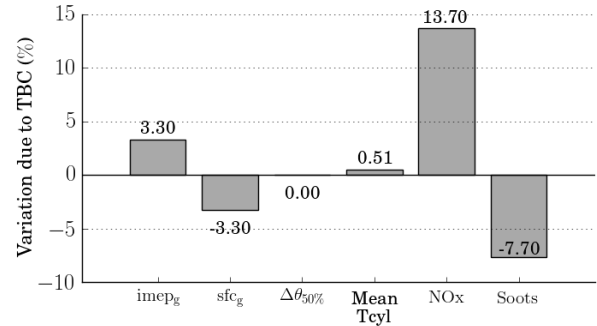
This last definition gives indications about the relative importance of each coated wall for the total insulation. The results of the liner are given here because they enter in the calculation of the evolution of the total heat losses, even though coating was not applied on its surface. All coated surfaces of the chamber see their heat losses decrease between 14.4 to 28.7%, giving a heat insulation rate over the chamber of 16.3%. Due to its large surface and its close contact with the hot gases, the piston TBC is responsible for nearly 75% of the total heat insulation rate (with an almost equal impact of the top and cavity parts, respectively 35 and 30%). The coating on the cylinder head represents 26.4%, and as for the valve bottoms TBC, it accounts for 5% of the total heat insulation rate. However, due to the absence of contact modeling between the valves and the head, the results of these surfaces have to be considered with caution.

The decrease in heat losses indicated in Fig. 14 is directly reflected in the performance and pollutant results of the engine, as shown in Fig. 15. As the combustion speed remains constant with TBC, the increased heat insulation results in an increase in imep_g of 3.3% (with a decrease in sfc_g of the same rate). The higher in-cylinder gas temperature (+0.51%) has an impact on the pollutants: this favors the production of NOx (+13.7%) as well as the post-oxidation of soots (-7.7%). The values of NOx and soot emissions however remains low, of the order of 0.50 g/kW.h.

Overall, these simulations show an improvement of 3.3% in gross indicated mean effective pressure and gross specific fuel consumption for a 100 μm-thick coating deposit in the entire combustion chamber, with a thermal conductivity of 0.4 $W \cdot m^{-1} \cdot K^{-1}$ and a volumetric heat capacity of 920 $kJ \cdot m^{-3} \cdot K^{-1}$. These results are among the most positive concerning the effect of recent TBCs, although it is not easy to compare results of setup which largely differ, in terms of engine characteristics, operating points and coating properties. However, a clear limitation of the present simulation is the negligence of the coating thermal inertia, for matters of computational cost. Thus, the objective of the

Figure 14. Heat insulation rate due to coating compared to baseline wall (dark grey) and compared to global heat losses decrease (light grey). ILVS: intake lower valve surface; ELVS: exhaust lower valve surface.

Figure 15. Variations in % of gross imep and sfc, $\Delta\Theta_{50\%}$, mean cylinder gas temperature and mass of NOx and soots at the start of exhaust for the case with TBC compared to the baseline.

next section is to evaluate the impact of this assumption on the results.

Uncertainty induced by the wall insulation model

In order to evaluate the impact of the coating thermal inertia, the 1D heat conduction solver presented previously was adapted to simulate a coating without thermal inertia, i.e. with a null volumetric heat capacity. One-dimensional simulations were conducted for three cases:

(i) no coating (baseline),
(ii) coating of thickness $e = 100\mu m$,
(iii) coating of thickness $e = 100\mu m$ with no thermal inertia.

The convective boundary condition representing the gas side, (h, T_{cyl}) is provided by the 3D CHT simulation (without coating). To improve the accuracy of the results, the 1D simulations are conducted with two different heat transfer coefficients $h_{dome}(CAD)$ and $h_{cavity}(CAD)$, computed over the piston dome and cavity of the 3D CHT simulation. This gives, for all three cases, two wall surface temperatures (at $x = 0$): $T_{dome}(CAD)$ and $T_{cavity}(CAD)$. These temperature profiles are then used as boundary conditions for three 3D CFD simulations (without CHT modeling). This is a way to overcome an important limitation of the 1D model previously mentioned, as the impact of wall surface temperature on in-cylinder gas will be taken into account in the 3D CFD simulations. For simplification and to represent for cases (ii) and (iii) a thermal insulation

over the entire piston, the temperature surface of the piston top is taken equal to the cavity surface temperature: $T_{cavity}(CAD) = T_{top}(CAD)$. The temperature profiles of all other surfaces are provided by the 3D CHT simulation. This chain of 1D and 3D simulations is illustrated in Fig. 16. Comparing the resulting 3D CFD simulations will give insight about the role of the coating thermal inertia when applied to the piston, in terms of heat insulation rate and engine performance. Finally, a 3D CHT simulation was run with TBC on the piston only, with the same assumption of no thermal inertia for the coating. The results of this simulation are compared to the baseline 3D CHT, and aim to validate the chain of 1D/3D simulations.

The effect of the TBC thermal inertia appears clearly when comparing the heat losses rate and cumulative heat losses across the piston surface for the three 1D/3D simulations, as illustrated in Fig. 17 for the piston dome. During the combustion phase, heat losses predicted by the simulation with a TBC with no thermal inertial ($\rho C_p = 0$) are largely lower than these predicted by the case modeling the coating thermal inertia. Focusing on heat losses accumulated during the intake phase (right plot in Fig. 17), it is clear that neglecting the coating thermal inertia will decrease the heat transfers from wall to gas during intake compared to the baseline. On the contrary, taking it into account will increase these heat transfers, therefore heating the air and decreasing the volumetric efficiency. These aspects are confirmed in Fig. 18, showing the variation of integrated heat transfer from wall to gas during intake and of the in-cylinder mass before SOI (start of injection) for the two coating models. Fig. 18 shows that an increase by 17.2% in heat transfer from the chamber walls to gas during intake is obtained when modeling the TBC thermal inertia, leading to a decrease in in-cylinder mass before SOI of -0.62%. Without the TBC thermal inertia, the increase in heat transfers drops to 4.1% (it is not negative as all walls of the chamber are considered here, not only the coated piston). This gives a decrease of the in-cylinder mass of -0.14%. The effect of the coated piston modeled in 3D CHT is close to those of the 1D/3D simulation with no thermal inertial, with almost no impact of the TBC on volumetric efficiency.

As for the heat insulation rate due to coating, Fig. 19 confirms that it is over-estimated (by roughly 10%) if the coating thermal inertia is neglected: the 1D/3D simulations with TBC at $\rho C_p = 0$ gives 24.6% of heat insulation over the piston (12.8% if all chamber walls are considered), against 15.2% if thermal inertia is modeled (7.5% over all chamber walls). This leads to an over-estimation of gain in $imep_g$ (and sfc_g in similar rates) if thermal inertia is not modeled, as illustrated in Fig. 20: +2.1% instead of +1.6%. As the in-cylinder gas temperature is slightly misestimated without TBC thermal inertial, the production of NOx and soot is logically impacted (keeping in mind that the values of emissions remain small). Finally, Figs. 19 and 20 show that the 3D CHT simulation with TBC on the piston gives similar results compared to the 1D/3D simulation with TBC and $\rho C_p = 0$. The heat insulation rates for both models, in particular, compare very well. This comforts the use of the 1D/3D simulations to evaluate the impact of the coating on engine performance and pollutants.

Overall, the gain to be expected for a coating on the piston surface for this operating point are limited: +1.6% in $imep_g$, (less than 0.2 bar), -1.6% in sfc_g, with an increase in NOx and decrease in soots due to the increase in in-cylinder gas temperature. These figures are coherent with recent results. For instance, a decrease in fuel consumption between -0.4 and -1.9% was found in a previous study[17] for a coating on various location on the piston.
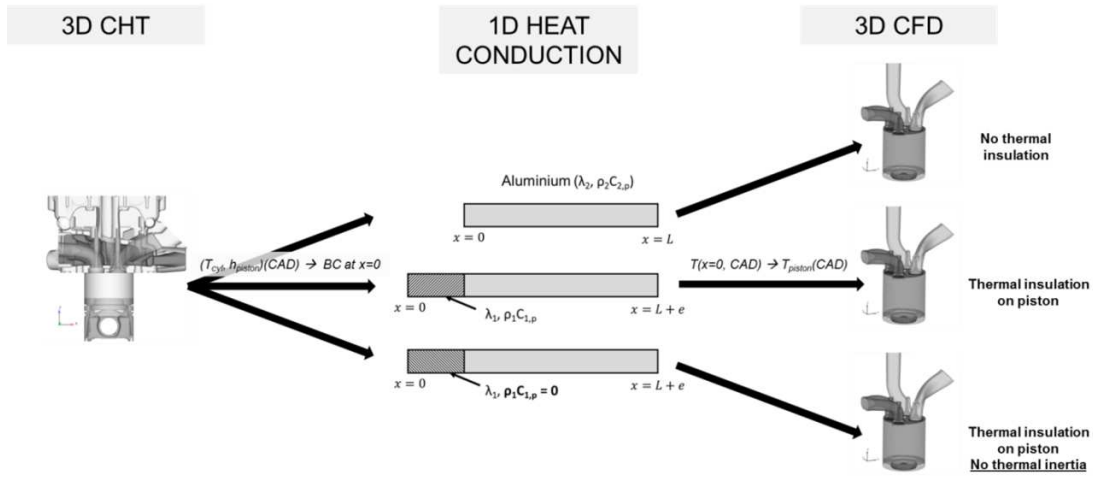
Based on these results, it is unreasonable to expect a decrease in fuel consumption of -3.3% for a coating on all chamber walls, as previously obtained with the 3D CHT simulation. However, it is possible to give a crude estimation of the gain to be expected for this case assuming that, like for the piston, modeling thermal inertia would take down the heat insulation rate of the cylinder head by about 10% (so from 24.4% in Fig. 14 to 14.4%). For a coating on the cylinder head, this represents 6J per cycle not lost in heat transfer. For all the simulations presented in this manuscript, about 65% of the energy not lost in heat transfers due to coating is converted to indicated work. Using this conversion ratio adds about 4J to the indicated work of the 1D/3D simulation with TBC on the piston, giving a decrease in fuel consumption of -2.1% for a coating on piston and cylinder head.
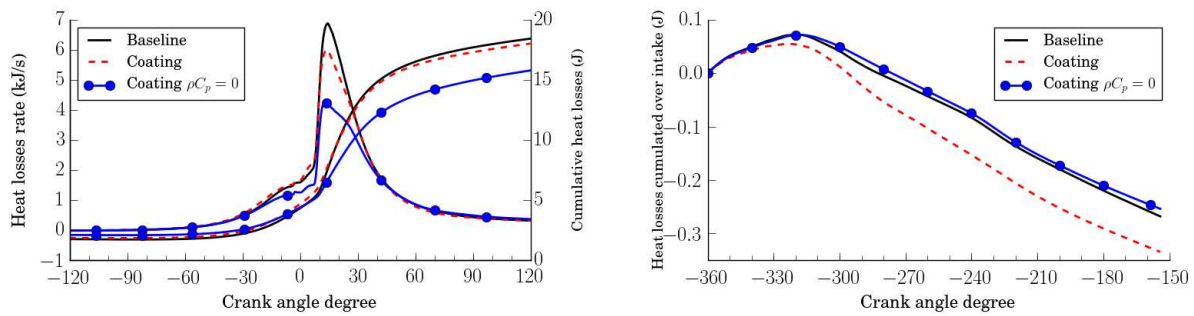
Conclusion

The present paper had a double objective:

(i) assessing a coupled in-cylinder/CHT methodology to model the effect of a coating deposit on the combustion chamber wall of a Diesel engine,

(ii) estimating the maximum gain to be expected from an innovative coating material by applying it on the entire surface of the combustion chamber.
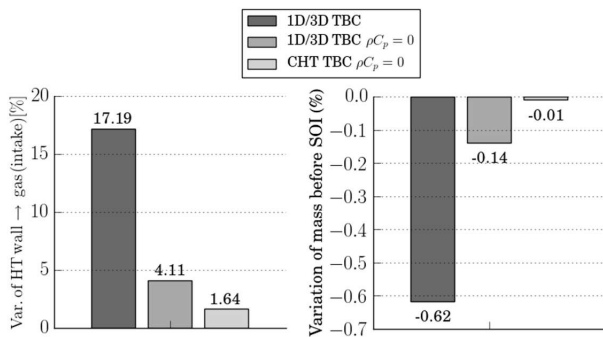
First, a 3D-RANS simulation of a single-cylinder Diesel engine, coupled with CHT of the engine cylinder head and piston, was presented. This setup, simulated for one operating point (2500 rpm for an imep of 12 bar), showed good comparison with measurements of in-cylinder pressure and apparent heat release rate. A similar configuration was then run to evaluate the impact of a 100 μm-thick layer of coating over all the combustion chamber walls (except the liner). The coating material, which is expected to act like a thermo-swing insulation according to 1D simulations, was modeled by a contact resistance, neglecting its thermal inertia. Results show a decrease of 3.3% in fuel consumption with a positive impact on volumetric efficiency. The average in-cylinder temperature is increased by 0.5%, resulting in a slight increase in NOx and decrease in soot emissions. These encouraging results, which concern a single operating point, are challenged by the absence of the coating thermal inertia in the model. A chain of 1D/3D simulations was implemented to be able to compare three cases: a baseline simulation without coating and two simulations modeling a 100 μm deposit of coating on the piston with and without its thermal inertia. The results show clearly an over-estimation of the heat insulation rate on the piston by about 10% when thermal inertia is not modeled (24.6% instead of 15.2%), as well as an over-estimation of the volumetric efficiency as the negligence of the coating
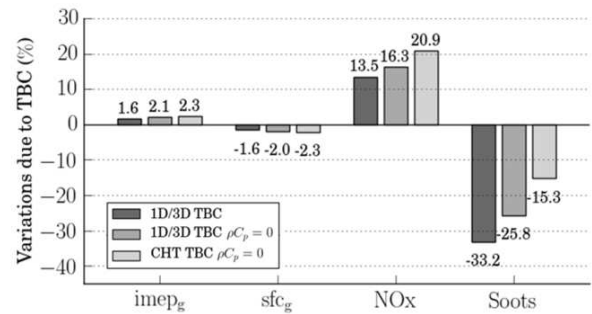
Figure 16. Chain of 1D/3D simulations to evaluate the impact of the coating thermal inertia.
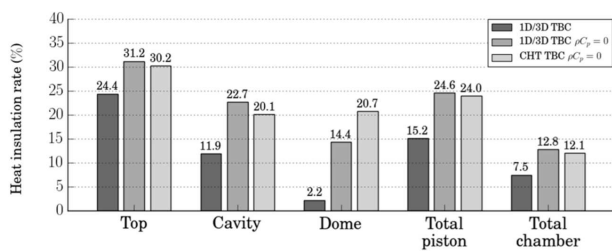

Figure 17. Heat losses rate and cumulative heat losses across the piston dome during a cycle (left), and heat losses accumulated during intake (right) obtained with the 1D/3D simulations.

Figure 18. Relative variation due to TBC on piston compared to the baseline of integrated heat transfer from wall to gas during intake (left) and of in-cylinder mass before SOI (right).

Figure 20. Relative variations due to TBC on piston of gross imep and sfc and of quantities of NOx and soots at the start of exhaust, compared to the baseline.

Figure 19. Heat insulation rate due to TBC on piston compared to the baseline.

thermal inertia leads to less air heating during intake. Logically, this results in an over-estimation of the gain in fuel

consumption due to coating on the piston: -2.0% instead of -1.6%. Based on these results, the gain in fuel consumption which could be expected with a coating on all chamber walls (except liner) was crudely estimated to -2.1%. It is important to keep in mind that only one operating point was considered in the present work, and that the gains would be different for other conditions. Overall, if the coupled 3D-RANS/CHT methodology appears promising to evaluate thermal boundary coatings in Diesel engine, efforts must be made to model the coating thermal inertia without impacting dramatically the computational cost, otherwise the gain brought by the coating will not be correctly estimated. The 1D/3D simulations, by modeling the coating thermal inertia,

offered a more sensible estimation of the coating effects. Future work should also take into account other aspects of the coating, like roughness, which certainly impact gas mixing and pollutant formation.

Acknowledgements

Declaration of conflicting interests

The author declares no potential conflicts of interest with respect to the research, authorship, and/or publication of this article.

Funding

Notes

1. The intake phase corresponds to the interval between intake valve opening and closing with a minimum lift at 0.2 mm, as indicated in Table 1.

References

1. Borman G and Nishiwaki K. Internal-combustion engine heat transfer. *Progress in Energy and Combustion Science* 1987; 13(1): 1–46. DOI:10.1016/0360-1285(87)90005-0.

2. Jia, M, Gingrich, E, Wang, H, Li, Y, Ghandhi, JB, and Reitz, RD. Effect of combustion regime on in-cylinder heat transfer in internal combustion engines. *International Journal of Engine Research* 2016; 17(3): 331–346. DOI:10.1177/1468087415575647.

3. Miyairi Y. Computer Simulation of an LHR DI Diesel Engine. *SAE Technical Paper* 1988; 880187. DOI:10.4271/880187.

4. Pawar AN, Jajoo BN and Nandgaonkar MR. Combustion analysis and performance of low heat rejection diesel engine with different thermal insulation coating. *SAE Technical Paper* 2004; 2004-28-0012. DOI:10.4271/2004-28-0012.

5. Tamilporai P, Baluswamy N, Jawahar PM et al. Simulation and Analysis of Combustion and Heat Transfer in Low Heat Rejection Diesel Engine Using Two Zone Combustion Model and Different Heat Transfer Models. *SAE Technical Paper* 2003; 2003-01-1067. DOI:10.4271/2003-01-1067.

6. Anderson DD. The Effects of Ceramic Port Insulation on Cylinder Head Performance in a Diesel Engine. *SAE Technical Paper* 1996; 961745. DOI:10.4271/961745.

7. Saad D, Saad P, Kamo L et al. Thermal Barrier Coatings for High Output Turbocharged Diesel Engine. *SAE Technical Paper* 2007; 2007-01-1442. DOI:10.4271/2007-01-1442.

8. Tovell JF. The Reduction of Heat Losses to the Diesel Engine Cooling System. *SAE Technical Paper* 1983; 830316. DOI:10.4271/830316.

9. Afify EM and Klett DE. The Effect of Selective Insulation on the Performance, Combustion, and NO Emissions of a DI Diesel Engine. *SAE Technical Paper* 1996; 960505. DOI:10.4271/960505.

10. Morel T, Fort EF and Blumberg PN. Effect of Insulation Strategy and Design Parameters on Diesel Engine Heat Rejection and Performance. *SAE Technical Paper* 1985; 850506. DOI:10.4271/850506.

11. Morel T, Keribar R, Blumberg PN et al. Examination of Key Issues in Low Heat Rejection Engines. *SAE Technical Paper* 1986; 860316. DOI:10.4271/860316.

12. Thring RH. Low Heat Rejection Engines. *SAE Technical Paper* 1986; 860314. DOI:10.4271/860314.

13. Dickey DW. The Effect of Insulated Combustion Chamber Surfaces on Direct-Injected Diesel Engine Performance, Emissions and Combustion. *SAE Technical Paper* 1989; 890292. DOI:10.4271/890292.

14. Morel T, Wahiduzzaman S and Fort EF. Heat Transfer Experiments in an Insulated Diesel. *SAE Technical Paper* 1988; 880186. DOI:10.4271/880186.

15. Binder C, Abou Nada F, Richter M et al. Heat Loss Analysis of a Steel Piston and a YSZ Coated Piston in a Heavy-Duty Diesel Engine Using Phosphor Thermometry Measurements. *SAE Int J Engines* 2017; 10(4). DOI:10.4271/2017-01-1046.

16. Caputo S, Millo F, Cifali G et al. Numerical Investigation on the Effects of Different Thermal Insulation Strategies for a Passenger Car Diesel Engine. *SAE Int J Engines* 2017; 10(4). DOI:10.4271/2017-24-0021.

17. Kawaguchi A, Iguma H, Yamashita H et al. Thermo-Swing Wall Insulation Technology; - A Novel Heat Loss Reduction Approach on Engine Combustion Chamber -. *SAE Technical Paper* 2016; 2016-01-2333. DOI:10.4271/2016-01-2333.

18. Fukui K, Wakisaka Y, Nishikawa N et al. Development of Instantaneous Temperature Measurement Technique for Combustion Chamber Surface and Verification of Temperature Swing Concept. *SAE Technical Paper* 2016; 2016-01-0675. DOI:10.4271/2016-01-0675.

19. Kawaguchi A, Iguma H, Yamashita H et al. Engine Heat Loss Reduction by Thermo-Swing Wall Insulation Technology: Mechanism Analysis and Effect on Low Temperature Starting. In *The Ninth International Conference on Modeling and Diagnostics for Advanced Engine Systems (COMODIA 2017)*. Okayama, Japan.

20. Kosaka H, Wakisaka Y, Nomura Y et al. Concept of "Temperature Swing Heat Insulation" in Combustion Chamber Walls, and Appropriate Thermo-Physical Properties for Heat Insulation Coat. *SAE Int J Engines* 2013; 6(1): 142–149. DOI:10.4271/2013-01-0274.

21. Wakisaka Y, Inayoshi M, Fukui K et al. Reduction of Heat Loss and Improvement of Thermal Efficiency by Application of "Temperature Swing" Insulation to Direct-Injection Diesel Engines. *SAE Int J Engines* 2016; 9(3). DOI:10.4271/2016-01-0661.

22. Uchihara K, Ishii M, Nakajima H et al. A Study on Reducing Cooling loss in a Partially Insulated Piston for Diesel Engine. *SAE Technical Paper* 2018; 2018-01-1276. DOI:10.4271/2018-01-1276.

23. Osada H, Watanabe H, Onozowa Y et al. Experimental Analysis of Heat-Loss with Different Piston Wall Surface Conditions in a Heavy-Duty Diesel Engine. In *The Ninth International Conference on Modeling and Diagnostics for Advanced Engine Systems (COMODIA 2017)*. Okayama, Japan.

24. Uchida N and Osada H. A New Piston Insulation Concept for Heavy-Duty Diesel Engines to Reduce Heat Loss from the Wall. *SAE Int J Engines* 2017; 10(5). DOI:10.4271/2017-24-0161.

25. Serrano JR, Arnau FJ, Martin J et al. Analysis of Engine Walls Thermal Insulation: Performance and Emissions.

SAE Technical Paper 2015; 2015-01-1660. DOI:10.4271/2015-01-1660.

26. Fujimoto H, Yamamoto H, Fujimoto M et al. A Study on Improvement of Indicated Thermal Efficiency of ICE Using High Compression Ratio and Reduction of Cooling Loss. *SAE Technical Paper* 2011; 2011-01-1872. DOI:10.4271/2011-01-1872.

27. De Paola, G, Rabeau, F, Knop, V, Willems, W. Modelling investigation of design approaches for Low Heat Rejection Diesel Engines. In *SIA Powertrain (2016)*. Rouen, France.

28. Cicalese G, Berni F, Fontanesi S et al. A Comprehensive CFD-CHT Methodology for the Characterization of a Diesel Engine: from the Heat Transfer Prediction to the Thermal Field Evaluation. *SAE Technical Paper* 2017; 2017-01-2196. DOI:10.4271/2017-01-2196.

29. Kundu P, Scarcelli R, Som S et al. Modeling Heat Loss through Pistons and Effect of Thermal Boundary Coatings in Diesel Engine Simulations using a Conjugate Heat Transfer Model. *SAE Technical Paper* 2016; 2016-01-2235. DOI:10.4271/2016-01-2235.

30. Leguille M, Ravet F, Le Moine J et al. Coupled Fluid-Solid Simulation for the Prediction of Gas-Exposed Surface Temperature Distribution in a SI Engine. *SAE Technical Paper* 2017; 2017-01-0669. DOI:10.4271/2017-01-0669.

31. Senecal, P, Richards, K, Pomraning, E, Yang, T, Dai, MZ, McDavid, R M, Patterson, M A, Hou, S, Shethaji, T. A New Parallel Cut-Cell Cartesian CFD Code for Rapid Grid Generation Applied to In-Cylinder Diesel Engine Simulations. *SAE Technical Paper* 2007; 2007-01-0159.

32. Colin O and Benkenida A. The 3-zones extended coherent flame model (ecfm3z) for computing premixed/diffusion combustion. *Oil & Gas Science and Technology* 2004; 59(6): 593–609. DOI:10.2516/ogst:2004043.

33. Colin O, Benkenida A and Angelberger C. 3D Modeling of Mixing, Ignition and Combustion Phenomena in Highly Stratified Gasoline Engines. *Oil & Gas Science and Technology* 2003; 58(1): 47–62. DOI:10.2516/ogst:2003004.

34. Knop V, Michel JB and Colin O. On the use of a tabulation approach to model auto-ignition during flame propagation in SI engines. *Applied Energy* 2011; 88(12): 4968–4979. DOI:10.1016/j.apenergy.2011.06.047.

35. Colin O, Pires da Cruz A and Jay S. Detailed chemistry-based auto-ignition model including low temperature phenomena applied to 3-D engine calculations. *Proceedings of the Combustion Institute* 2005; 30(2): 2649–2656. DOI:10.1016/j.proci.2004.08.058.

36. Curran HJ, Gaffuri P, Pitz WJ et al. A Comprehensive Modeling Study of n-Heptane Oxidation. *Combustion and Flame* 1998; 114(1-2): 149–177. DOI:10.1016/S0010-2180(97)00282-4.

37. Bohbot J, Colin O, Velghe A et al. An Innovative Approach Combining Adaptive Mesh Refinement, the ECFM3Z Turbulent Combustion Model, and the TKI Tabulated Auto-Ignition Model for Diesel engine CFD Simulations. *SAE Technical Paper* 2016; 2016-01-0604. DOI:10.4271/2016-01-0604.

38. Hiroyasu H and Kadota T. Models for Combustion and Formation of Nitric Oxide and Soot in Direct Injection Diesel Engines. *SAE Technical Paper* 1976; 760129. DOI:10.4271/760129.

39. Zeldovitch YAB, Sadovnikov PYA, Frank-Kamenetskii DA. Oxidation of Nitrogen in Combustion: translated by M. Shelef. *Academy of Science of USSR, Moscow* 1947; .

40. Launder BE and Spalding DB. The numerical computation of turbulent flows. *Computer Methods in Applied Mechanics and Engineering* 1974; 3(2): 269–289. DOI:10.1016/0045-7825(74)90029-2.

41. Amsden AA. KIVA-3V: A Block-Structured KIVA Program for Engines with Vertical or Canted Valves. Technical report, Los Alamos National Laboratory Report, 1997.

42. Reitz RD and Diwakar R. Structure of High-Pressure Fuel Sprays. *SAE Technical Paper* 1987; 870598. DOI:10.4271/870598.

43. O'Rourke PJ and Amsden AA. A Spray/Wall Interaction Submodel for the KIVA-3 Wall Film Model. *SAE Technical Paper* 2000; 2000-01-0271. DOI:10.4271/2000-01-0271.

44. Kogo T, Hamamura Y, Nakatani K et al. High Efficiency Diesel Engine with Low Heat Loss Combustion Concept - Toyota's Inline 4-Cylinder 2.8-Liter ESTEC 1GD-FTV Engine -. *SAE Technical Paper* 2016; 2016-01-0658. DOI:10.4271/2016-01-0658.

45. Andruskiewicz P, Najt P, Durrett R et al. Analysis of the effects of wall temperature swing on reciprocating internal combustion engine processes. *International Journal of Engine Research* 2018; 19(4): 461–473. DOI:10.1177/1468087417717903.